Available online at www.sciencedirect.com
ScienceDirect
Journal of Sound and Vibration 324 (2009) 1003–1015
JOURNAL OF SOUND AND VIBRATION
www.elsevier.com/locate/jsvi

The effect of modal energy transfer on the sound radiation and vibration of a curved panel: Theory and experiment

Y.Y. Lee[a,*], R.K.L. Su[b], C.F. Ng[c], C.K. Hui[a]

[a]Department of Building and Construction, City University of Hong Kong, Kowloon Tong, Kowloon, Hong Kong
[b]Department of Civil and Structural Engineering, Hong Kong Polytechnic University, Hung Hom, Kowloon, Hong Kong
[c]Department of Civil Engineering, The University of Hong Kong, Pokfulam Road, Hong Kong

Received 15 November 2008; received in revised form 18 February 2009; accepted 28 February 2009
Handling Editor: L.G. Tham
Available online 1 April 2009

Abstract

This study is the first work to consider the sound radiation of a panel subject to 2:1 internal resonance. The research also furthers the experimental work of a previous paper that did not make use of 2:1 internal resonance for sound reduction and failed to tune the frequency ratio of the first symmetric and anti-symmetric modes of the curved structure close to two. The results indicate that when the ratio of the resonant frequencies of the first bending symmetric and anti-symmetric modes is close to two, and the excitation frequency is equal to the resonant frequency of the first symmetric mode, the contribution of the first anti-symmetric mode is significant, even though the curved panel and excitation are symmetrical. This is because a large amount of the vibration energy is transferred to the anti-symmetric mode, whose sound radiation efficiency is much lower than that of the symmetric mode. Thus, the total sound radiated from the panel is reduced.

1. Introduction

The dynamics of nonlinear systems have been widely investigated in various research studies. For example, Yamaki et al. [1,2] examined the effects of axial displacement on the dynamic responses of a clamped beam and the corresponding internal and combination resonances. Abou-Rayan et al. [3] performed a theoretical study of the nonlinear single-mode responses of a simply supported curved beam to parametric excitation, and Feng and Hu [4] presented their nonlinear beam work using the multi-mode approach. Other studies have considered the two-mode responses of various systems with internal resonance (e.g., [5]), but have not examined the coupling between the symmetric and anti-symmetric modes. Some studies of two-to-one internal resonance (e.g., [6–8]) have shown that the anti-symmetric modes of a curved panel can be excited by symmetric excitations, and Nayfeh and Mook [9] presented a detailed theoretical and experimental discussion of the two-to-one internally resonant responses of a beam-mass system. However, only limited results have been obtained regarding the effects of internal resonance on sound radiation. Lee et al. [10] considered the

*Corresponding author. Tel.: +852 2788 9847; fax: +852 2788 9643, 2788 7612.
E-mail address: bcraylee@cityu.edu.hk (Y.Y. Lee).

0022-460X/$ - see front matter © 2009 Elsevier Ltd. All rights reserved.
doi:10.1016/j.jsv.2009.02.042

effects of the anti-symmetric mode on the total vibration response of a curved beam, but failed to tune the frequency ratio of the first symmetric and anti-symmetric modes closer to two. The theoretical and experimental work in this study investigated the effects of 2:1 internal resonance on the noise and vibration responses of curved structures.

2. Theory

Consider an initially curved panel or shallow shell that is simply supported or clamped at two opposite sides and free at the other two, and is subject to transverse harmonic base excitation (see Fig. 1). In our theoretical model, flexural bending along the width is neglected. Thus, this structure can be considered to be a beam-like panel. The governing differential equation of a curved beam that is subject to uniform base harmonic excitation [11] is given by

$$\rho A\ddot{w} + \Omega\dot{w} + EIw'''' = \frac{EA}{L}(w'' + \overline{w}'')\int_0^L \left(\overline{w}'w' + \frac{1}{2}(w')^2\right)\mathrm{d}x - F\sin\omega t, \tag{1}$$

where w is the transverse displacement caused by the panel bending; $\dot{w}$ and $\ddot{w}$ the first and second derivatives of the transverse displacement with respect to time t; w', w'', and w'''' the first, second, and fourth derivatives of the transverse displacement with respect to the spatial variable, x; $\overline{w}$ the initial transverse displacement of the panel; E Young's modulus of the panel; ρ the material density of the panel; Ω the damping coefficient of the panel; $A = B \times h$ the cross-sectional area of the panel; B panel width; h panel thickness; L panel length; F the base excitation amplitude (where $F = \rho A g \kappa$); ω the excitation frequency; κ the base excitation parameter; and g the gravity $= 9.81\,\mathrm{ms}^{-2}$.

Consider that the transverse displacement is expressed in terms of the panel mode shapes

$$w(x,t) = \sum_{i=1}^{N} q_i(t)\phi_i(x), \tag{2}$$

where q_i is the modal amplitude of the ith mode; ϕ_i the ith mode shape, which is normalized so that the maximum value of each mode shape is equal to one; i the mode number; and N the number of modes considered.

It is assumed that the initial deflection shape $\overline{w} = q_0\phi_1$, where q_0 is the transverse displacement at the center. Hence, the residual can be defined by substituting Eq. (2) into (1), as follows.

$$\begin{aligned}\Delta = {} & \rho A\sum_{i=1}^{N}\ddot{q}_i\phi_i + \xi\omega_i\sum_{i=1}^{N}\dot{q}_i\phi_i + EI\sum_{i=1}^{N}q_i\phi_i'''' - \frac{EA}{L}\left(\sum_{i=1}^{N}q_i\phi_i'' + q_0\phi_1''\right)\\ & \times\left(\sum_{i=1}^{N}q_0q_i\int_0^L\phi_1'\phi_i'\,\mathrm{d}x + \frac{1}{2}\sum_{i=1}^{N}\sum_{j=1}^{N}q_iq_j\int_0^L\phi_i'\phi_j'\,\mathrm{d}x\right) + F\sin\omega t\end{aligned} \tag{3}$$

where ϕ_i', ϕ_i'', and ϕ_i'''' the first, second and fourth derivatives of the ith mode shape, respectively and i, j the mode numbers. $\xi\omega_i = \Omega$, where $\xi =$ modal damping coefficient.

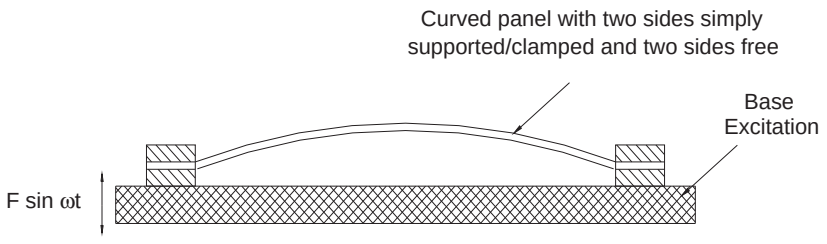

Fig. 1. Side view of a curved panel under base excitation.

Using the Galerkin approach [12], the weighted residual in Eq. (3) is set to zero. Multiplying ϕ_m by each term on the right-hand side of Eq. (3) and taking the integration over the beam length gives

$$\rho A\sum_{i=1}^{N}\ddot{q}_i\alpha_{i,m}^{0,0}+\xi\omega_i\sum_{i=1}^{N}\dot{q}_i\alpha_{i,m}^{0,0}+EI\sum_{i=1}^{N}q_i\alpha_{i,m}^{4,0}-\frac{EA}{L}\left[+\sum_{i=1}^{N}\alpha_{1,i}^{1,1}\alpha_{1,m}^{2,0}q_0^2q_i\right.$$
$$\left.+\sum_{i=1}^{N}\sum_{j=1}^{N}\left(\alpha_{1,i}^{1,1}\alpha_{j,m}^{2,0}+\frac{1}{2}\alpha_{i,j}^{1,1}\alpha_{1,m}^{2,0}\right)q_0q_iq_j+\frac{1}{2}\sum_{i=1}^{N}\sum_{j=1}^{N}\sum_{k=1}^{N}\alpha_{i,j}^{1,1}\alpha_{k,m}^{2,0}q_iq_jq_k\right]-\ddot{q}_{b,m}=0, \tag{4}$$

where $\beta_m=\int_0^L\phi_m\,\mathrm{d}x$; $\alpha_{i,m}^{0,0}=\int_0^L\phi_i\phi_m\,\mathrm{d}x$; $\alpha_{i,m}^{2,0}=\int_0^L\phi_i''\phi_m\,\mathrm{d}x$; $\alpha_{i,m}^{4,0}=\int_0^L\phi_i''''\phi_m\,\mathrm{d}x$; $\alpha_{i,m}^{1,1}=\int_0^L\phi_i'\phi_m'\,\mathrm{d}x$; m, k the mode numbers, $\ddot{q}_{b,m}$ the modal base acceleration $=F\beta_m\sin\omega t/\rho A\alpha_{m,m}^{0,0}$.

Similarly, multiplying another mode shape function by Eq. (4) and taking the integration allows $\mathrm{N}\times\mathrm{N}$ matrix equations to be set up. The unknown modal amplitude, $|q_i|$, can be solved using Runge–Kutta time domain numerical integration.

Note that the linear modal stiffness terms in Eq. (4) are

$$K_{i,m}=EI\alpha_{i,m}^{4,0}-\frac{EA}{L}\alpha_{1,i}^{1,1}\alpha_{1,m}^{2,0}q_0^2. \tag{5}$$

For the simply supported condition, the mode shapes are obviously given by

$$\phi_m(x)=\sin\left(\frac{m\pi x}{L}\right). \tag{6}$$

Hence, by substituting Eq. (6) into (5), the linear modal stiffness matrix becomes diagonal, i.e.,

$$K_{i,m}=0\quad\text{for } i\neq m. \tag{7}$$

For the clamped condition, the mode shapes must satisfy the following boundary conditions.

$$\phi_m(x)=\phi_m'(x)=0\quad\text{at } x=0 \text{ or } L. \tag{8}$$

To have linear diagonal modal stiffness and the mass matrices in Eq. (4), the mode shapes are also required to satisfy the following conditions.

$$\int_0^L\phi_m\phi_i\,\mathrm{d}x=0\quad\text{for } i\neq m; \tag{9a}$$

$$\int_0^L\phi_m''''\phi_i\,\mathrm{d}x=0\quad\text{for } i\neq m; \tag{9b}$$

$$\int_0^L\phi_1'\phi_i'\,\mathrm{d}x=0\quad\text{for } 1\neq i; \tag{9c}$$

$$\int_0^L\phi_1''\phi_m\,\mathrm{d}x=0\quad\text{for } 1\neq m;\ \text{and} \tag{9d}$$

$$\int_0^L\phi_1''\phi_i\,\mathrm{d}x=0\quad\text{for } 1\neq i. \tag{9e}$$

Let the symmetrical mode shapes for the clamped panel be

$$\phi_m(x)=\frac{1}{C_m}\sum_{s=1}^{S_m}C_{m,s}\psi_s(x), \tag{10}$$

where $\psi_s(x)=(1-\cos((2\pi s/L)x))$ is a "sub-mode shape" that is able to satisfy the boundary conditions in Eq. (8); $C_{m,s}$ is set to one, whereas the other coefficients, $C_{m,s}$, are unknowns to be determined; C_m is a normalization constant so that the maximum value of ϕ_m is equal to one; and S_m is the number of sub-mode shapes used. By substituting Eq. (10) into (9a–e), a set of equations can be set up and used to solve for the

unknown coefficients $C_{m,s}$. The total number of sub-mode shapes is selected according to the condition that the number of equations is equal to the number of unknown coefficients $C_{m,s}$. Then, the anti-symmetric mode shapes are given by

$$\phi_m(x) = \frac{1}{C_m}\left(\cosh(\gamma_m x) - \cos(\gamma_m x) - \frac{\cos(\gamma_m L) - \cosh(\gamma_m L)}{\sin(\gamma_m L) - \sinh(\gamma_m L)}(\sinh(\gamma_m x) - \sin(\gamma_m x))\right), \tag{11}$$

where γ_m is the mth root of the equation $\cosh(\gamma L)\cos(\gamma L) - 1 = 0$; the anti-symmetric mode shapes in Eq. (11) are adopted from the exact solution to the clamped beam. Note that the mode shape in Eq. (11) satisfies the conditions in Eqs. (8) and (9a–e).

As previously mentioned, the modal amplitudes can be found in the time-domain numerical integration. The modal vibration and acoustic energies of each mode can also be found and are proportional to $|\dot{q}_m^2|$, which represents the temporal average of the square of the response of the mth mode. Thus, the modal vibration energy contribution ratio, the normalized modal vibration energy, and the normalized total vibration energy are given by

$$D_{v,m} = \frac{|\dot{q}_m^2|}{\sum_{i=1}^{N}|\dot{q}_i^2|}, \tag{12a}$$

$$E_{v,m} = 10\log\frac{|\dot{q}_m^2|}{G} \tag{12b}$$

$$E_v = 10\log\frac{\sum_m|\dot{q}_m^2|}{G}, \tag{12c}$$

where G is a normalization constant so that the maximum values of $E_{v,m}$ and E_v are equal to one.

Similarly, the modal contribution ratio of the acoustic energy radiated from the vibrating panel, the normalized modal sound energy, and the normalized total sound energy are given by

$$D_{s,m} = \frac{|\dot{q}_m^2|\sigma_m}{\sum_{i=1}^{N}|\dot{q}_i^2|\sigma_i}, \tag{13a}$$

$$E_{s,m} = 10\log\frac{|\dot{q}_m^2|\sigma_m}{G}, \tag{13b}$$

$$E_s = 10\log\frac{\sum_m|\dot{q}_m^2|\sigma_m}{G}, \tag{13c}$$

where σ_m is the radiation efficiency of the mth mode (the calculation of the acoustic pressure radiated from a vibrating panel is described in the following paragraph).

It is noted that Eqs. (12)–(13) consider the flexural vibration amplitudes of the panel only. The predictions for the modal vibration, total vibration, modal sound, and total sound energies of the vibrating panel plus the excitation base are computed by

$$E'_{v,m} = 10\log\frac{|(\dot{q}_m + \dot{q}_{b,m})^2|}{G}, \tag{14a}$$

$$E'_v = 10\log\frac{\sum_m|(\dot{q}_m + \dot{q}_{b,m})^2|}{G}, \tag{14b}$$

$$E'_{s,m} = 10\log\frac{|(\dot{q}_m + \dot{q}_{b,m})^2|\sigma_m}{G}, \tag{14c}$$

$$E'_s = 10\log\frac{\sum_m|(\dot{q}_m + \dot{q}_{b,m})^2|\sigma_m}{G}. \tag{14d}$$

The resulting acoustic pressure at an observer point $P_m(r,\phi,\varphi)$, which is radiated from the mth vibrating mode shape of a panel, can be found from the modified Rayleigh's integral [12] and is given by

$$P_m(r,\theta,\varphi) = -i_0 k_0 \rho_0 c_0 \frac{e^{i_0 k_0 r}}{2\pi r} \int_0^B \int_0^L \phi_m e^{-i_0(\gamma x/L+\eta y/B)}\,dx\,dy. \tag{15a}$$

Hence, the sound power radiated from the mth mode and the sound radiation efficiency are given by

$$\Pi_m = \int_0^{2\pi} \int_0^{\pi/2} \frac{|P_m(r,\theta,\varphi)|^2}{\rho_0 c_0} r^2 \sin(\theta)\,d\theta\,d\varphi, \tag{15b}$$

$$\sigma_m = \frac{8\Pi_m}{\rho_0 c_0 BL}, \tag{15c}$$

where σ_m is the sound radiation efficiency of the mth mode; Π_m the sound power from the mth mode; $|P_m(r,\phi,\varphi)|$ the acoustic pressure magnitude at the observer point; γ the $k_0 L \sin\theta\cos\varphi$; η the $k_0 B \sin\theta \sin\varphi$; r the distance between the panel corner and the observer point; θ and φ the angle between r and the y-axis and the angle between r and the x-axis, respectively (see [12]); k_0 the wave number; ρ_0 and c_0 the air density and sound speed; respectively; and $i_0 = \sqrt{-1}$.

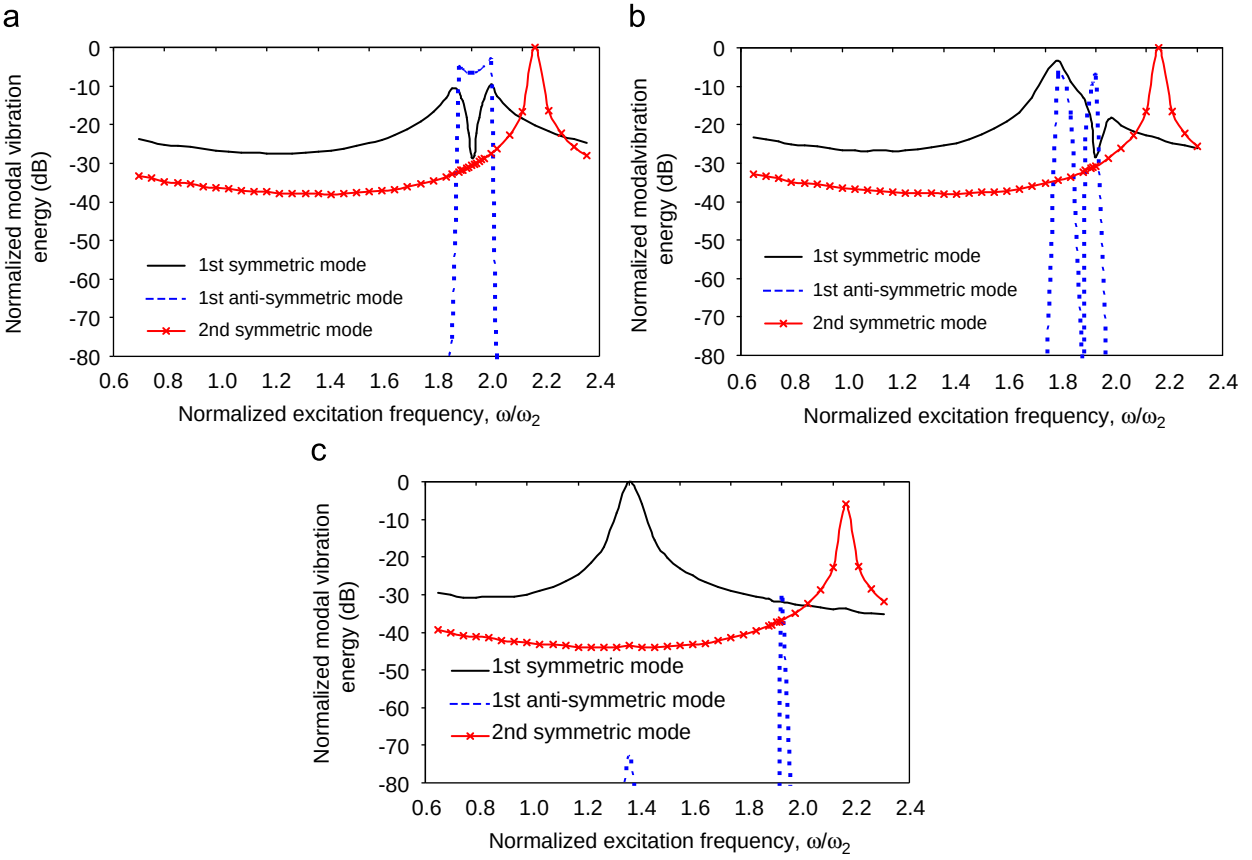

Fig. 2. (a) Theoretical normalized modal vibration energy of the simply supported panel ($\omega_1/\omega_2 = 2$). (b) Theoretical normalized modal vibration energy of the simply supported panel ($\omega_1/\omega_2 = 1.85$). (c) Theoretical normalized modal vibration energy of the simply supported panel ($\omega_1/\omega_2 = 1.43$).

3. Numerical results

In Fig. 2a, the normalized modal vibration energy of the simply supported panel is plotted against the normalized excitation frequency. The Young's modulus and density of the panel are $200\times10^9\,\mathrm{N/m^2}$ and $7800\,\mathrm{kg/m^3}$, respectively. The dimensions are $B=150\,\mathrm{mm}\times L=400\,\mathrm{mm}\times h=0.5\,\mathrm{mm}$. The initial center deflection, base excitation parameter and damping ratio are $\overline{w}=1.6\,\mathrm{mm}$, $\kappa=0.01$ and $\xi=0.02$, respectively. The resonant frequencies of the first symmetric and anti-symmetric modes are $\omega_1=2\omega_2$ and $\omega_2=2\pi\times28.702$ radian/s, respectively, and the resonant frequencies of the second symmetric and anti-symmetric modes are $\omega_3=2\pi\times64.579$ radian/s and $\omega_4=2\pi\times114.807$ radian/s, respectively. Figs. 2b–c show the normalized modal vibration energies for the cases that the initial center deflection of the panel is adjusted to $\overline{w}=1.5\,\mathrm{mm}$ and 1.15 mm, and the resonant frequency is adjusted to $\omega_1=1.85\omega_2$ and $\omega_1=1.43\omega_2$, respectively. In Fig. 2a, at a ω/ω_2 ratio close to 2 (where $\omega=$ the excitation frequency), the "V trough" on the solid line indicates a sharp reduction in the amplitude of the first symmetric mode. In contrast, the first anti-symmetric mode amplitude increases sharply and becomes highly significant. This phenomenon can be explained by the vibration energy transfer from the symmetric mode to the anti-symmetric mode. The peak at $\omega/\omega_2=2.25$ is caused by the resonance of the second symmetric mode. The line that represents the second anti-symmetric mode does not appear on the graph because its amplitude is very small and is outside the bounds of the figure. In Fig. 3a, there is a peak at $\omega/\omega_2=2$ on the dotted line, which represents the typical linear vibration

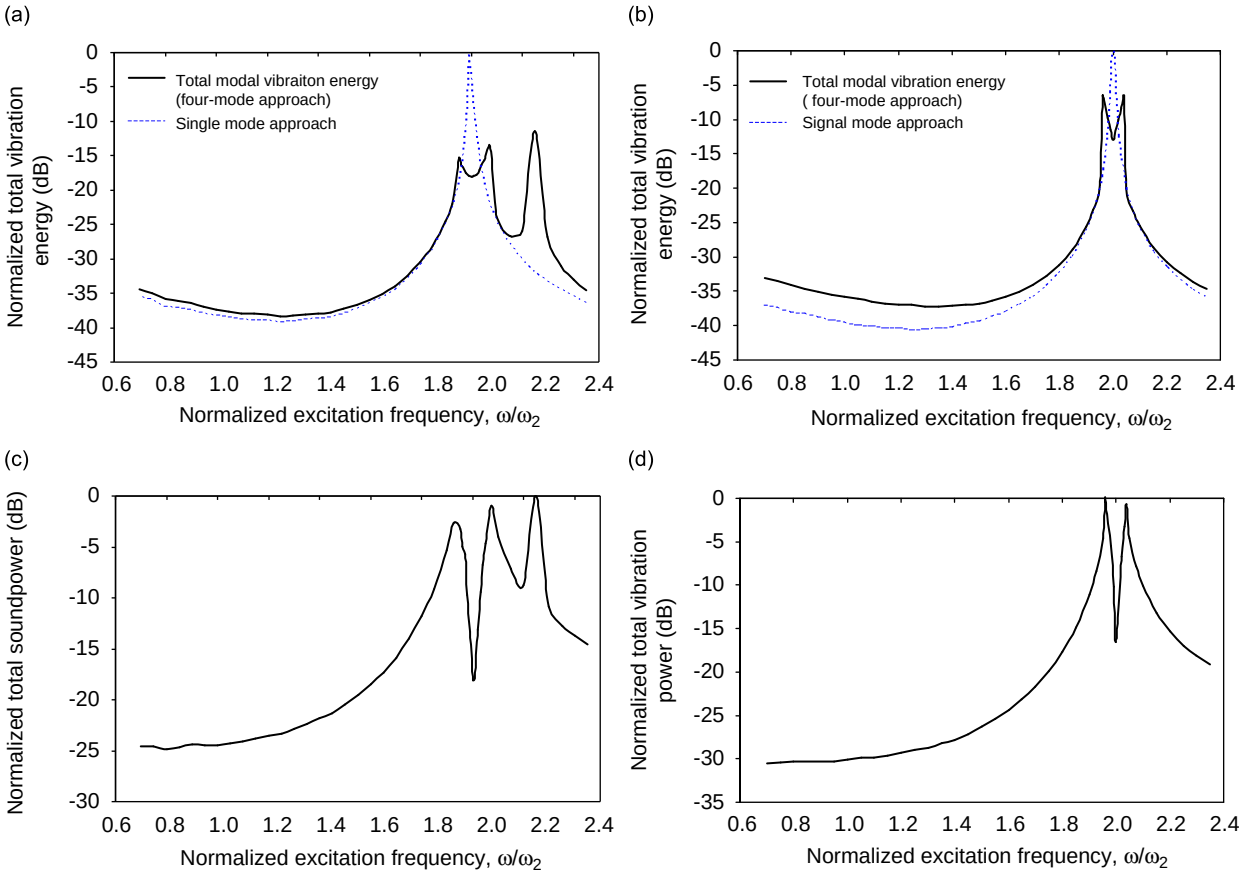

Fig. 3. (a) Theoretical normalized total vibration energy of the simply supported panel ($\omega_1/\omega_2=2$). (b) Theoretical normalized total vibration energy of the clamped panel ($\omega_1/\omega_2=2$). (c) Total sound energy radiated from the simply supported panel ($\omega_1/\omega_2=2$). (d) Total sound energy radiated from the clamped panel ($\omega_1/\omega_2=2$). (e) Sound radiation efficiency of the mode shapes of the simply supported panel. (f) Time histories of the modal responses of the simply support panel ($\omega/\omega_2=2$). (g) Frequency spectrums of the modal responses in Fig. 3f.

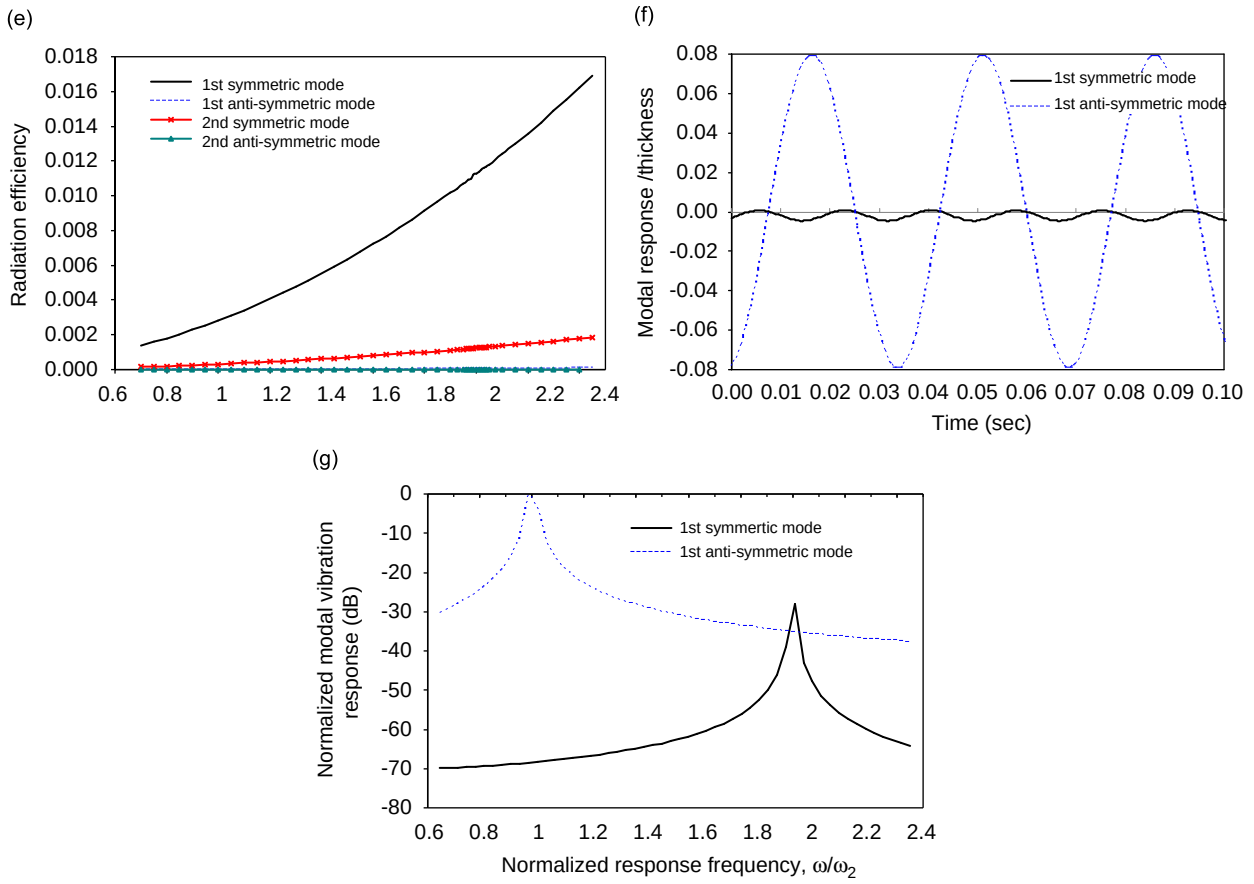

Fig. 3. (*Continued*)

phenomenon. The comparison between the two lines indicates that the single mode approach is incorrect and unable to prove the existence of the modal energy transfer. Similarly, in Figs. 2b–c, a "V trough" that is much smaller than that in Fig. 2a appears on the solid line around $\omega/\omega_2 = 2$. The first anti-symmetric mode amplitude increases sharply and becomes highly significant around $\omega/\omega_2 = 2$. The amplitude also jumps sharply at a ω/ω_2 close to 1.85 in Fig. 2b or 1.43 in Fig. 2c, but that of the first symmetric mode is much more significant. This implies that the modal energy transfers are very weak when compared with the case in Fig. 2a. It can be seen that a weaker modal energy transfer still exists if ω_1/ω_2 is close to 2.

In Figs. 3a–b, the normalized total vibration energies of the simply supported and clamped panels are plotted against the normalized excitation frequency. The material properties and configurations of the simply-supported panel are the same as those in Fig. 2a. For the clamped panel, the initial center deflection is $\overline{w} = 1.45$ mm; the other configurations and material parameters are also the same as those in Fig. 2a. In Figs. 3a–b, the peaks at $\omega/\omega_2 = 2$ on the dotted lines represent the typical linear vibration resonance, while the troughs at $\omega/\omega_2 = 2$ on the solid lines represent the aforementioned nonlinear modal coupling phenomenon. Thus, the comparison between the lines indicates that the single mode approach is incorrect and is unable to prove the existence of the modal energy transfer. In addition, it is observed that the energy transfer at $\omega/\omega_2 = 2$ in the case of the simply supported panel is more significant than in the case of the clamped panel. In Figs. 3c–d, the normalized total sound powers are plotted for the cases in Figs. 3a–b. Obviously, the sound contribution due to the first anti-symmetric mode is much less significant. This is because (1) at low to medium frequencies (or below the critical frequency), the radiation efficiency of the first anti-symmetric mode is much lower than that of the first symmetric mode (see Fig. 3e); and (2) the first anti-symmetric mode response frequency is only half of the first symmetric mode response frequency at $\omega/\omega_2 = 2$ (see the time domain modal responses and the corresponding frequency spectra in Figs. 3f–g). The radiation efficiencies in Fig. 3e are

Table 1
(a) Modal vibration energy contribution ratio for the simply supported panel at $\omega/\omega_2 = 2$. (b) Modal sound energy contribution ratio for the simply panel at $\omega/\omega_2 = 2$.

Contribution ratio	1 mode approach	2 mode approach	3 mode approach	4 mode approach
(a)				
1st symmetric mode, ω_1	100.000	0.630	0.628	0.628
1st anti-symmetric mode, ω_2	–	99.370	98.983	98.958
2nd symmetric mode, ω_3	–	–	0.389	0.389
2nd anti-symmetric mode, ω_4	–	–	–	0.025
(b)				
1st symmetric mode, ω_1	100.000	87.140	82.493	82.493
1st anti-symmetric mode, ω_2	–	12.860	12.174	12.174
2nd symmetric mode, ω_3	–	–	5.333	5.333
2nd anti-symmetric mode, ω_4	–	–	–	0.000

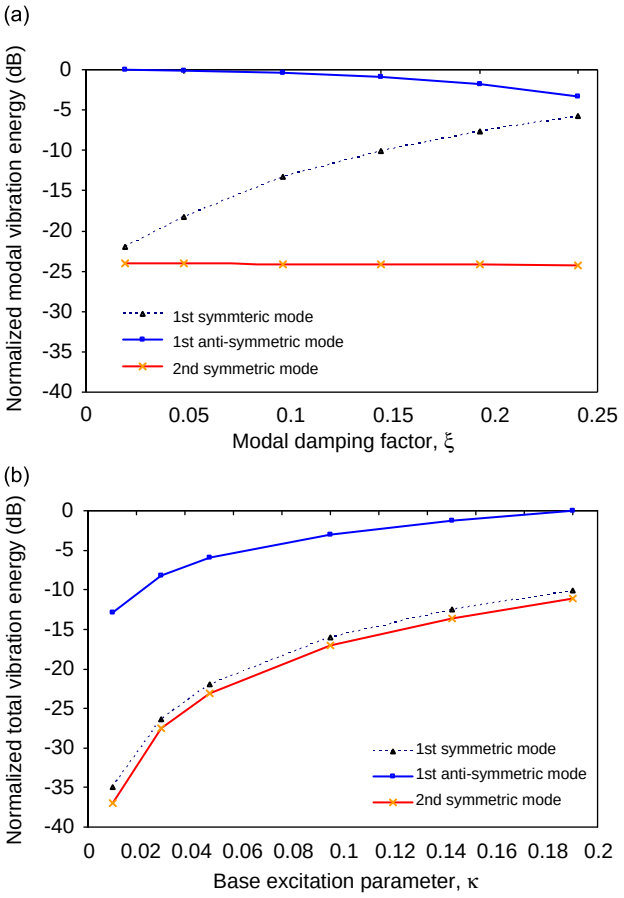

Fig. 4. (a) Theoretical normalized modal vibration energy of the simply supported panel vs the modal damping factor ($\omega/\omega_2 = 2$). (b) Theoretical normalized modal vibration energy of the simply supported panel vs the base excitation parameter ($\omega/\omega_2 = 2$).

calculated using Eqs. (15a–c). Thus, the lower response frequency of the first anti-symmetric mode leads to lower sound radiation. Tables 1a–b show the comparisons between the various modal acoustic and vibration energy contribution ratios at $\omega/\omega_1 = 2$ for the simply-supported panel. The three-mode approach is sufficient and is able to achieve five-digit accuracy.

In Fig. 4a, the normalized modal vibration energies of the simply supported panel are plotted against the damping ratio for $\omega/\omega_2 = 2$, and the panel configurations and parameters are the same as those in Fig. 2a. The first anti-symmetric mode vibration energy monotonically decreases for damping ratios from 0.01 to 0.25. Its vibration energy is the highest among the four modes considered. The first symmetric vibration level steadily increases for damping ratios from 0.01 to 0.25. Its vibration energy approaches that of the first anti-symmetric mode when the damping ratio is near 0.25. The second anti-symmetric mode and the second

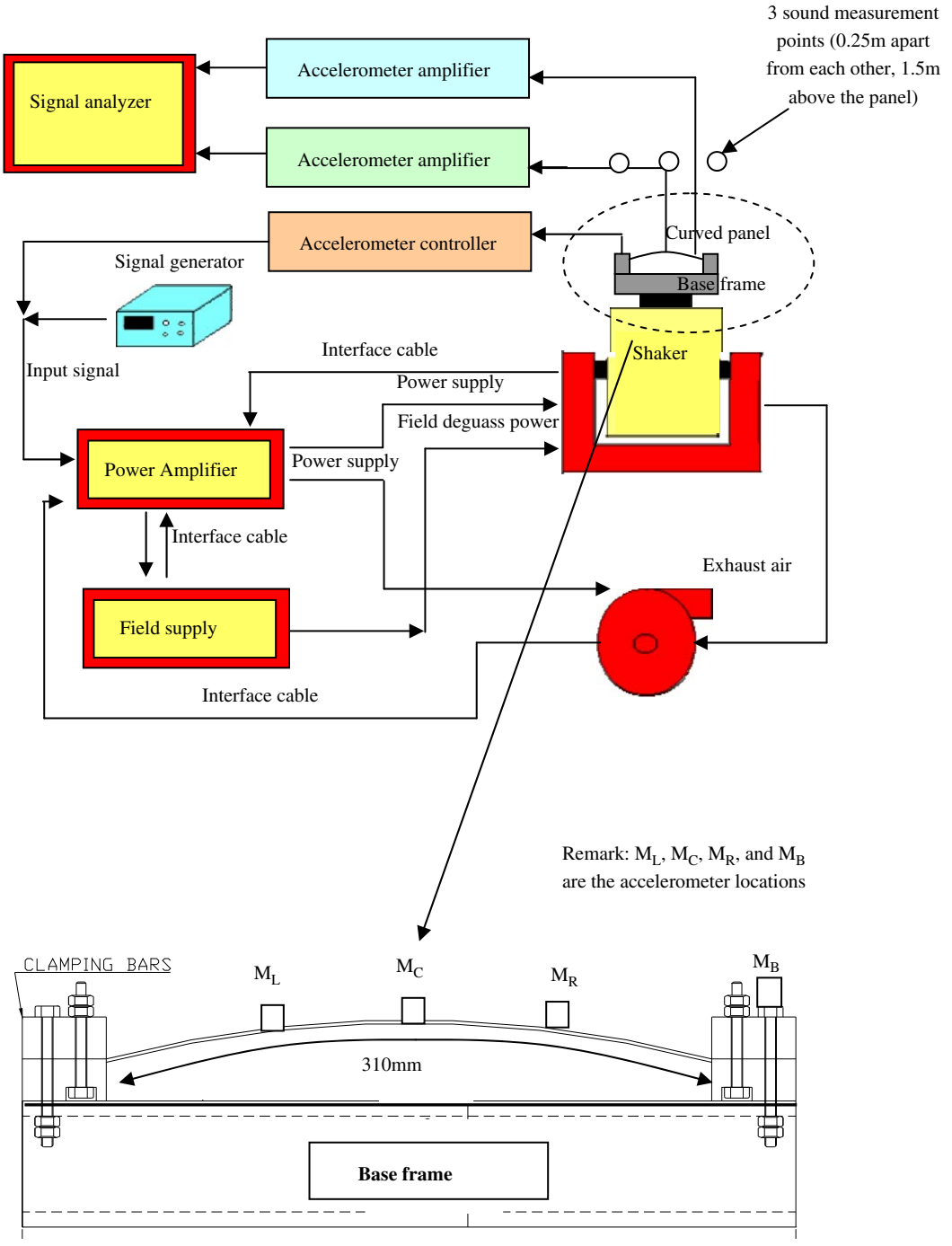

Fig. 5. The experimental setup.

symmetric mode vibration energy levels are nearly constant and not very significant. Fig. 4b plots the normalized vibration energies of the first symmetric mode, the first anti-symmetric mode and the second symmetric mode against the base acceleration factor for $\omega/\omega_2 = 2$. The other panel configurations and parameters are the same as those in Fig. 2a. All of the normalized vibration energies increase monotonically, and the first anti-symmetric mode always plays the most important role in the base acceleration range considered.

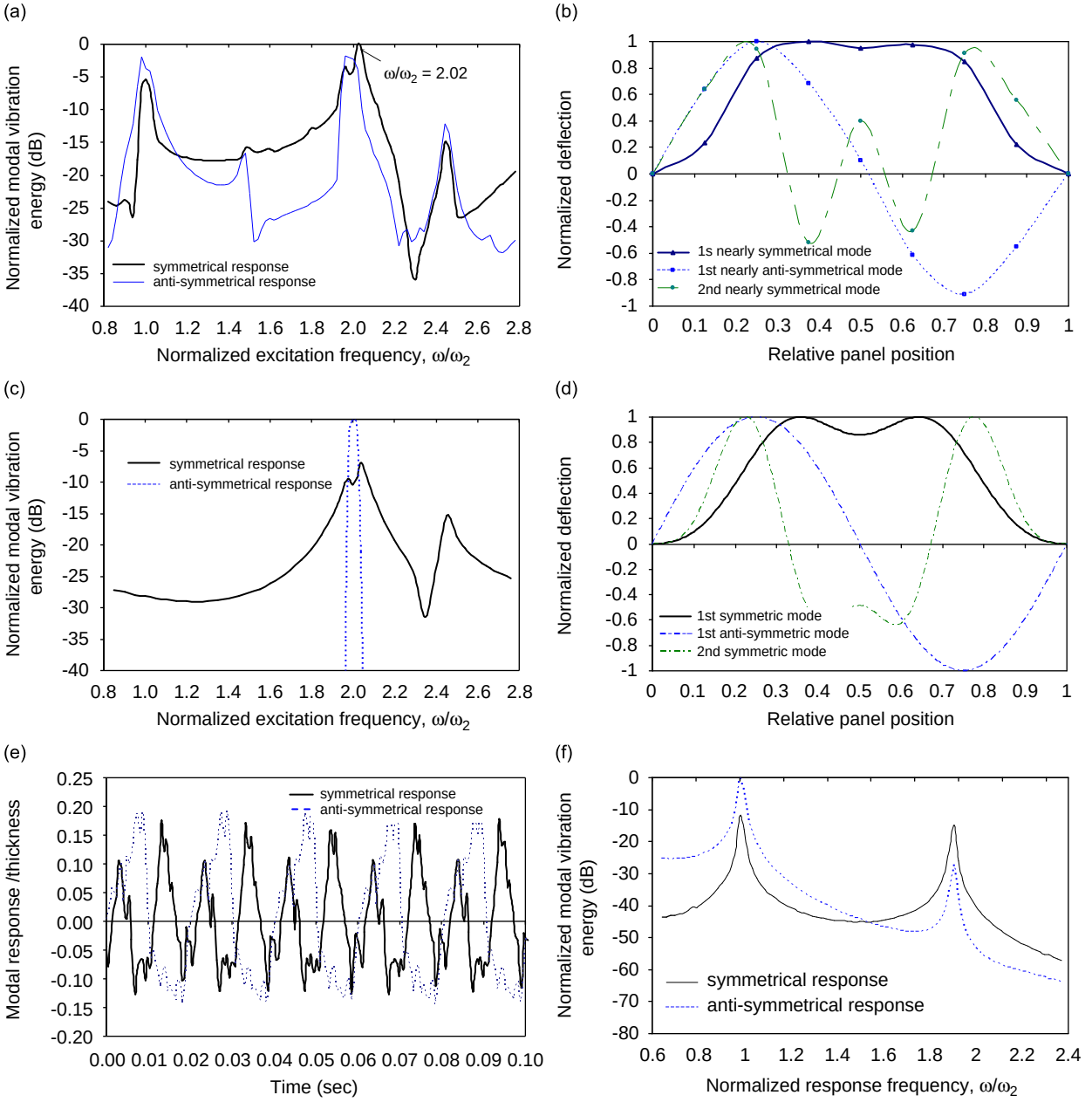

Fig. 6. (a) Experimental normalized modal vibration energy of the clamped steel panel ($\omega_1/\omega_2 = 2.02$). (b) Experimental mode shapes. (c) Theoretical normalized modal vibration energy of the clamped steel panel ($B = 150\,\text{mm}$; $L = 300\,\text{mm}$; $h = 0.5\,\text{mm}$; $\kappa = 0.175\,\text{g}$; $\xi = 0.04$; $\omega_1/\omega_2 = 2.02$). (d) Theoretical mode shapes. (e) Time histories of the modal responses of the clamped steel panel ($\omega/\omega_2 = 2.02$). (f) Frequency spectrums of the modal responses in Fig. 6e.

4. Experiment setup

A curved panel with a thickness of 0.5 mm, an arc length of 310 mm, and a breadth of 350 mm was fabricated from a steel sheet. Two sides of the panel were clamped, and the other two remained free. Note that the inevitable slipping effect at the clamped sides caused a deviation in the natural frequency response. Tests were conducted by periodically exciting the base frame and measuring the displacement of the panel from the frame using accelerometers as sensing elements. The test setup was similar to that in [10]. A schematic diagram of the complete setup is shown in Fig. 4. The base frame was bolted to the exciter table of a 6000-N electromagnetic vibration shaker, and a uniformly distributed pulsating load was applied to the panel by shaking the base frame sinusoidally. In the experiment, the two resonant frequencies were tuned to nearly 2 by placing a strut at the panel center and adjusting the curvature. The dynamic responses of the panel were obtained via accelerometers. An additional accelerometer was used to monitor the dynamic response of the shaker table. This arrangement allowed the frame to be subject to sine-wave excitation for a wide frequency range. Three microphones were also set 1.5 m above the panel surface to measure the average level of the sound that radiated from the panel. Note that the sound and vibration measurements were conducted in an anechoic chamber to ensure that the sound received by the microphones was mainly and directly from the panel vibration. The temporally averaged magnitudes of the total symmetrical and anti-symmetrical responses of the panel and the base excitation are defined by

$$\dot{q}_{\mathrm{sym}} = \sqrt{\frac{\sum_{j_*=1}^{M}(\dot{W}_{C,j_*})^2}{M}}; \quad \dot{q}_{\mathrm{ant}} = \sqrt{\frac{\sum_{j_*=1}^{M}\left(\frac{\dot{W}_{L,j_*}-\dot{W}_{R,j_*}}{2}\right)}{M}}; \quad \dot{q}_{\mathrm{bas}} = \sqrt{\frac{\sum_{j_*=1}^{M}(\dot{W}_{B,j_*})^2}{M}}, \tag{16a–c}$$

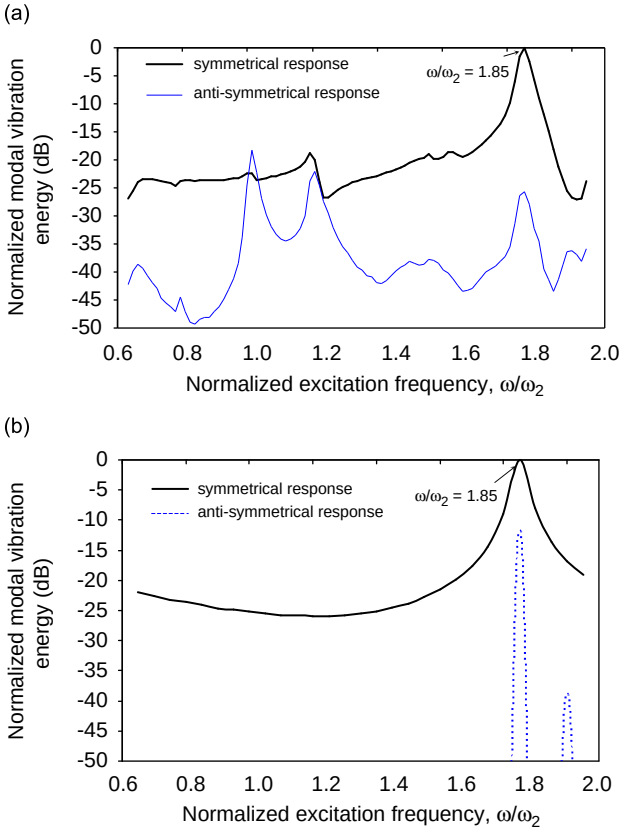

Fig. 7. (a) Experimental normalized modal vibration energy of the clamped steel panel ($\omega_1/\omega_2 = 1.85$). (b) Theoretical normalized modal vibration energy of the clamped steel panel ($B = 150$ mm; $L = 300$ mm; $h = 0.5$ mm; $\kappa = 0.05$; $\xi = 0.04$; $\omega_1/\omega_2 = 1.85$).

where W_{C,j_*}, W_{L,j_*}, W_{R,j_*}, and W_{B,j_*} are the dynamic responses at the j_*th time steps of the measurement locations, respectively, and M is the total time step (Fig. 5).

5. Experimental results and verifications

Fig. 6a depicts the experimental normalized modal vibration energy of the clamped curved panel under symmetrical base excitation ($\kappa = 0.175$, $\omega_1/\omega_2 = 2.02$). Fig. 6b shows the measured mode shapes. The first two modes are nearly symmetric (101 Hz) and anti-symmetric (50 Hz), respectively. As the panel was not perfectly symmetrical, a few anti-symmetrical responses were induced (see the experimental mode shapes in Fig. 6b). Significant resonant peaks can be found on the two curves at $\omega/\omega_2 = 1$, 2.02, and 2.43. Figs. 6c–d show the theoretical normalized modal vibration energies of the clamped curved panel and the mode shapes. The experimental and theoretical results indicate that the anti-symmetrical responses become very significant around $\omega_1/\omega_2 = 2.02$. The small resonant peaks on the experimental curves at $\omega/\omega_2 = 1.58$, which are caused by another panel mode, cannot be predicted by the beam model. In addition, there are two resonant peaks at $\omega/\omega_1 = 1$ on the experimental curves in Fig. 6a, but no similar peaks in Fig. 6c. These symmetrical and anti-symmetrical resonant responses at $\omega/\omega_2 = 1$ were induced in the experiment because of the unsymmetrical property of the beam. Figs. 6e–f show the time histories of the beam responses for $\omega/\omega_2 = 2.02$, and the corresponding frequency spectrums. The dominant frequencies of the anti-symmetric and symmetric responses are only half of, and the same as, the excitation frequency, respectively. This agrees with the theoretical results shown in Figs. 3f–g.

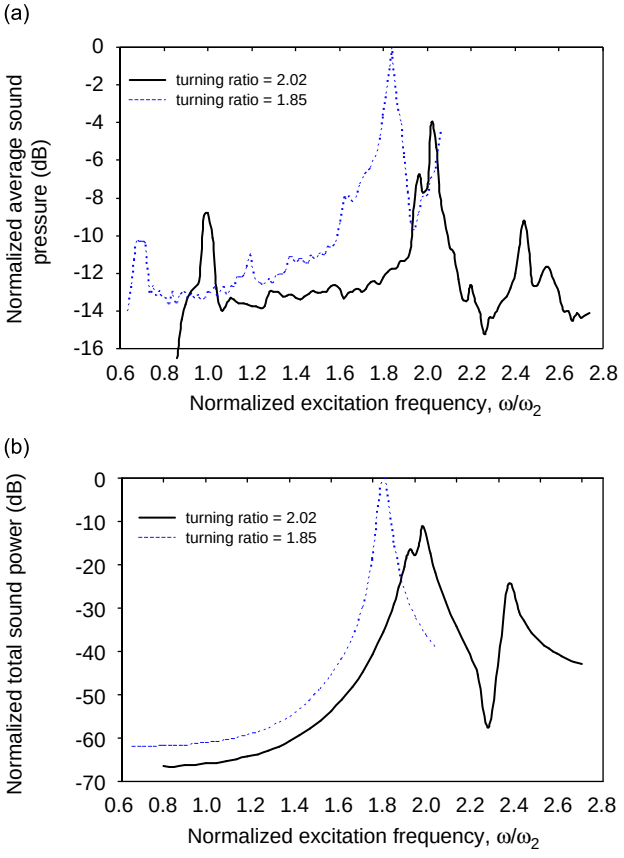

Fig. 8. (a) Experimental normalized total sound energy of the clamped steel panel. (b) Theoretical normalized total sound energy of the clamped steel panels in Figs. 6a and b.

Fig. 7a shows the experimental normalized modal vibration energy of the clamped curved panels ($\kappa = 0.175$, $\omega_1/\omega_2 = 126/68 = 1.85$). Generally, the symmetrical response is more significant than the anti-symmetrical response. No strong modal coupling can be found. This agrees with the theoretical prediction in Fig. 7b. Moreover, similar to those in Fig. 6a, the peaks at $\omega/\omega_2 = 1$ and 1.58 in Fig. 7a cannot be found in the theoretical prediction in Fig. 7b.

Figs. 8a–b depict the experimental and theoretical normalized total radiated sound levels of the clamped curved panel for $\omega_1/\omega_2 = 2.02$ and 1.85. These experimental and theoretical results indicate that the total radiated sound is significantly reduced when $\omega_1/\omega_2 = 2.02$, because energy transfer occurs from the high radiation symmetrical mode to the low radiation anti-symmetrical mode. The experimental data for $\omega_1/\omega_2 = 1.85$ was only recorded for the frequency range $\omega/\omega_2 = 0.62$ to 2.08. In addition, note that the sound power level predictions in Fig. 8b cannot be directly compared with the measured sound pressure levels in Fig. 8a.

6. Conclusion

This study demonstrated that anti-symmetric responses can be induced in a symmetrical curved panel under symmetric excitation, provided that the ratio of the resonant frequencies of the first bending symmetric and anti-symmetric modes is close to two, and that the excitation frequency is equal to the resonant frequency of the first symmetric mode (which are the main conditions for two-to-one internal resonance). The contribution of the first anti-symmetric mode to the total vibration response is highly significant, even though the curved panel and excitation distribution are symmetrical. This occurs because a large amount of the vibration energy is transferred to the anti-symmetric mode, the sound radiation efficiency of which is much lower than that of the symmetric mode. Hence, the overall sound radiated from the panel is reduced.

Acknowledgement

The work described in this paper was fully supported by a grant from the Hong Kong Research Grants Council [Project no. 9041239, CityU/115607]. The authors would like to express their sincere gratitude and appreciation to Dr. WY Poon for his advices about the experimental setup throughout this research.

References

[1] N. Yamaki, A. Mori, Non-linear vibrations of a clamped beam with initial defection and initial axial displacement, Part I theory, *Journal of Sound and Vibration* 71 (1980) 333–346.
[2] N. Yamaki, K. Otomo, A. Mori, Non-linear vibrations of a clamped beam with initial defection and initial axial displacement, Part II experiment, *Journal of Sound and Vibration* 71 (1980) 347–360.
[3] A.M. Abou-Rayan, A.H. Nayfeh, D.T. Mook, M.A. Nayfeh, Nonlinear response of a parametrically excited buckled beam, *Nonlinear Dynamics* 2 (1993) 499–525.
[4] Z.H. Feng, H.Y. Hu, Principal parametric and three-to-one internal resonances of flexible beams undergoing a large linear motion, *ACTA Mechanica Sinica* 19 (4) (2003) 355–364.
[5] D.T. Mook, R.H. Plaut, The influence of an internal resonance on non-linear structural vibrations under subharmonic resonance conditions, *Journal of Sound and Vibration* 102 (1985) 473–492.
[6] J.J. Thomsen, Chaotic vibrations of non-shallow arches, *Journal of Sound and Vibration* 153 (2) (1992) 239–258.
[7] H. Hatwal, A.K. Mallik, A. Ghosh, Non-linear vibrations of a harmonically excited autoparametric system, *Journal of Sound and Vibration* 81 (2) (1982) 153–164.
[8] A.G. Haddow, A.D.S. Barr, D.T. Mook, Theoretical and experimental study of modal interaction in a two-degree-of-freedom structure, *Journal of Sound and Vibration* 97 (3) (1984) 451–473.
[9] A.H. Nayfeh, D.T. Mook, *Nonlinear Oscillations*, Wiley Interscience, New York, 1979.
[10] Y.Y. Lee, W.Y. Poon, C.F. Ng, Anti-symmetric mode vibration of a curved beam subject to autoparametric excitation, *Journal of Sound and Vibration* 290 (2006) 48–64.
[11] W.Y. Poon, C.F. Ng, Y.Y. Lee, Dynamic stability of curved beam under sinusoidal loading, *Journal of Aerospace Engineering, Proceeding of the Institution of Mechanical Engineers—Part G* 216 (2002) 209–217.
[12] F. Fahy, *Sound and Structural Vibration-Radiation, Transmission and Response*, 6th ed., Academic Press, New York, 2000.